Supplementary Information (SI) for Sustainable Energy & Fuels.


*Supporting information*

# *Dopant Induced Enhanced Ion Diffusion in Flower-shaped Hollandite-$MnO_2$: Wearable Supercapacitor with Improved Energy Storage*

*Subin Kaladi Chondath[a], Love Bansal[a], Deb Kumar Rath[a], Nikita Ahlawat[a], Bhumika Sahu[a], Saumya Tiwari[b], Anjali Chaudhary[b], and Rajesh Kumar[a,c]**

[a]Department of Physics, Indian Institute of Technology Indore, Simrol-453552, India.

[b]Department of Physics, Indian Institute of Technology Bhilai-491002, India.

[c]Centre for advanced electronics, Indian Institute of Technology Indore, Simrol- 453552, India.

* Email: rajeshkumar@iiti.ac.in

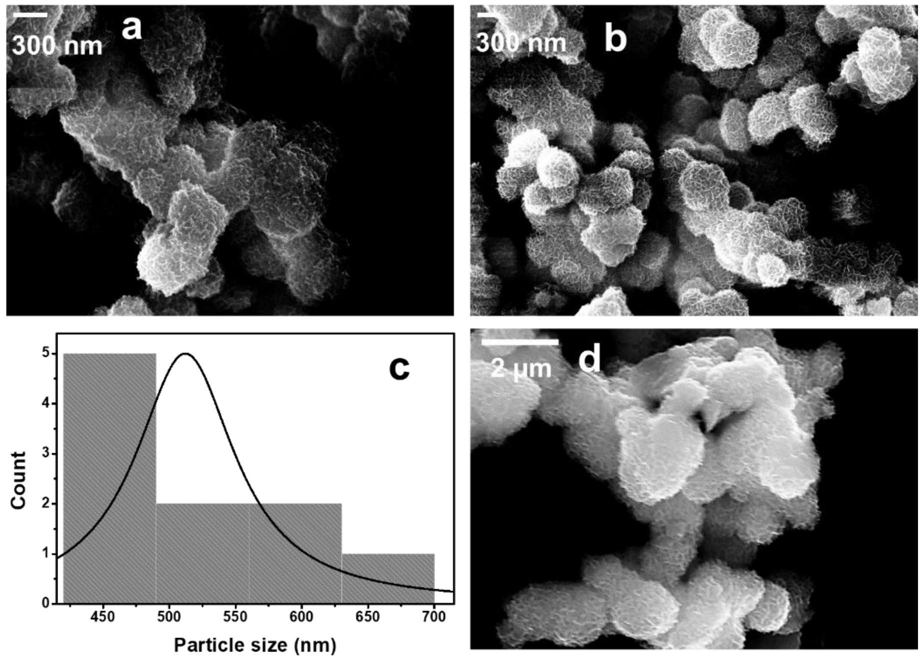


**Figure S1.** FESEM images of (a) $MnO_2$ and (b) NMO. (c) Histogram plot showing the particle size distribution of NMO flowers. (d) FESEM image acquired for elemental mapping.

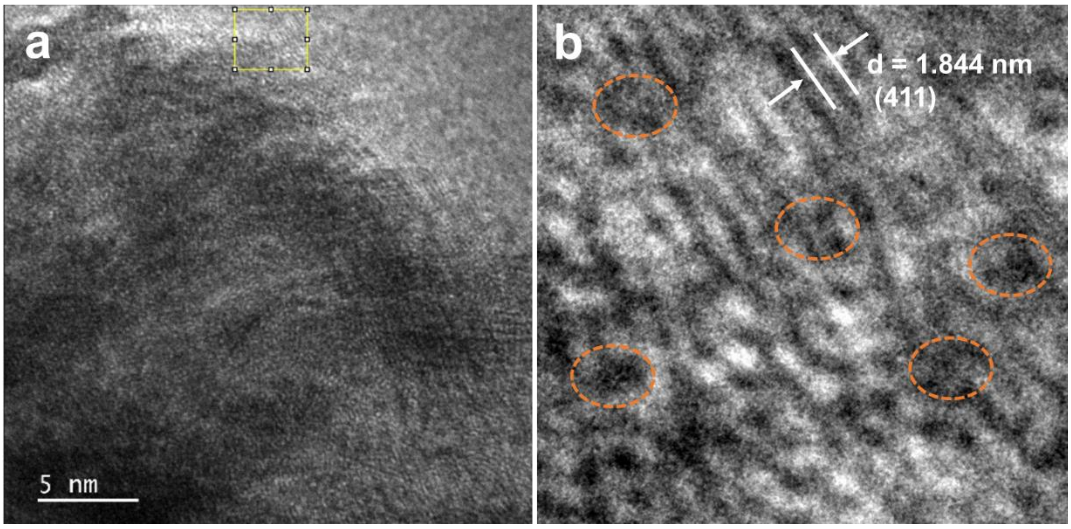


**Figure S2.** (a) High-magnification TEM image of NMO flowers with the marked region showing lattice fringes. (b) Zoomed portion showing lattice fringes indexed to (411) plane. Orange-circled regions show the twisted lattice fringes confirming lattice distortions.

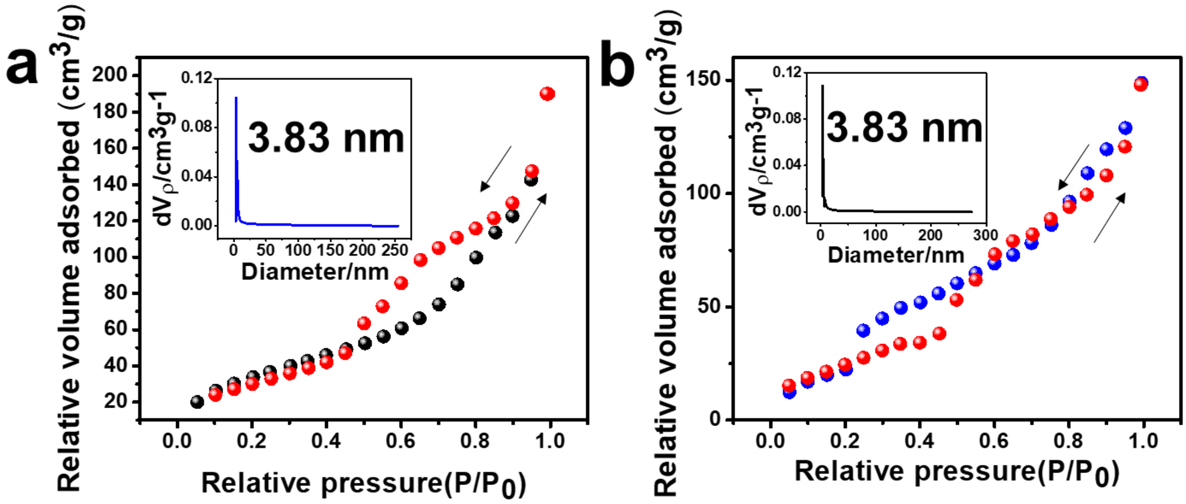


**Figure S3.** (a-b) $N_2$ adsorption-desorption isotherms of $MnO_2$ and NMO. The insets show the corresponding pore size distribution curves. The calculated pore size was 3.83 nm.

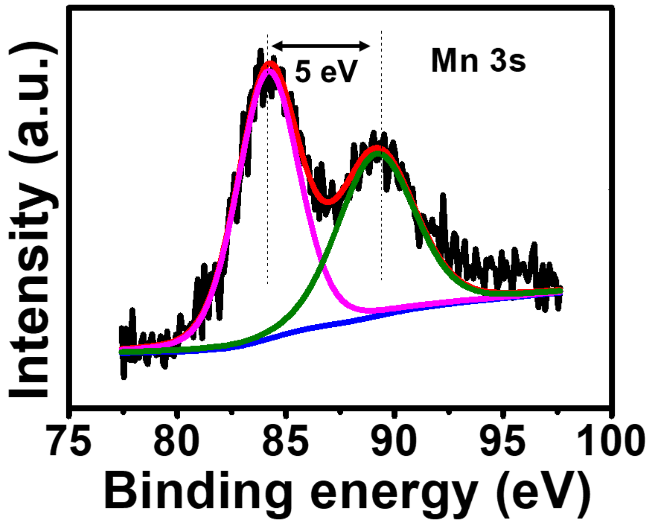


**Figure S4.** XPS spectrum of Mn 3s in NMO.

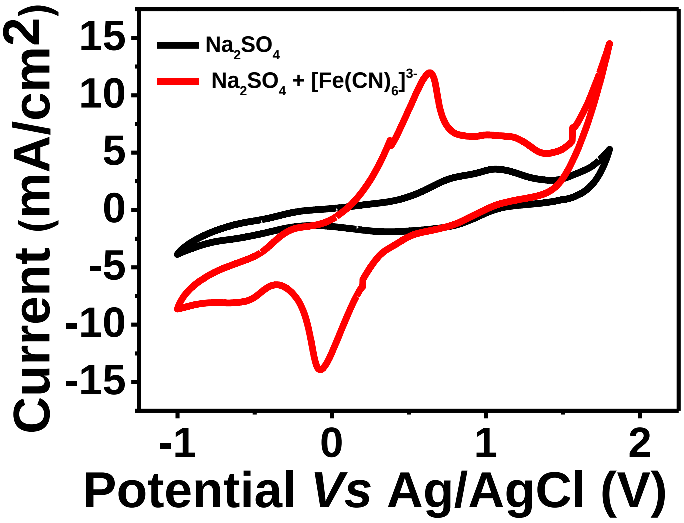


**Figure S5.** CV curves of $MnO_2$ with and without redox-additive electrolyte.

**Equations for calculating areal and gravimetric capacitance**

$$C_{areal} = \frac{I \times \Delta t}{A \times \Delta V} \text{ (} I \text{ in mA, } t \text{ in secs, } A \text{ in cm}^2\text{, and } V \text{ in volts),} \quad \text{(S1)}$$

$$C_{gravimetric} = \frac{I \times \Delta t}{m \times \Delta V} \text{ (} I \text{ in A, } t \text{ in secs, } m \text{ in grams, and } V \text{ in volts),} \quad \text{(S2)}$$

Here $C_{areal}$ in mF/cm$^2$ and $C_{gravimetric}$ in F/g represents the areal and gravimetric capacitance of the electrodes.

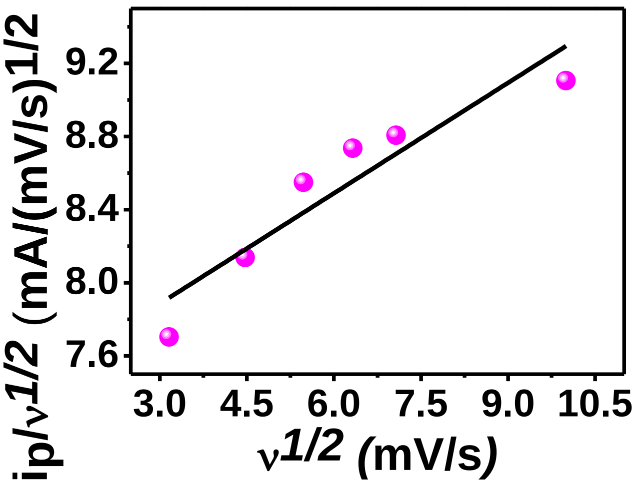


**Figure S6.** Plot between $\frac{i_p}{v^{1/2}}$ and $v^{1/2}$ at 1.2 V.

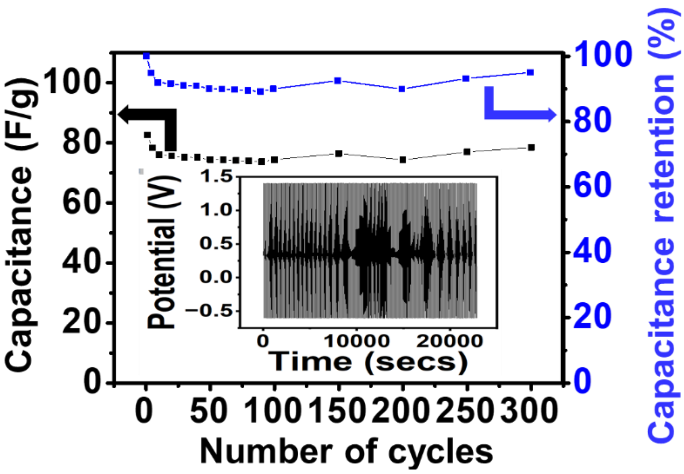


**Figure S7.** Plot showing the electrode stability and capacitance retention after 300 GCD cycles.

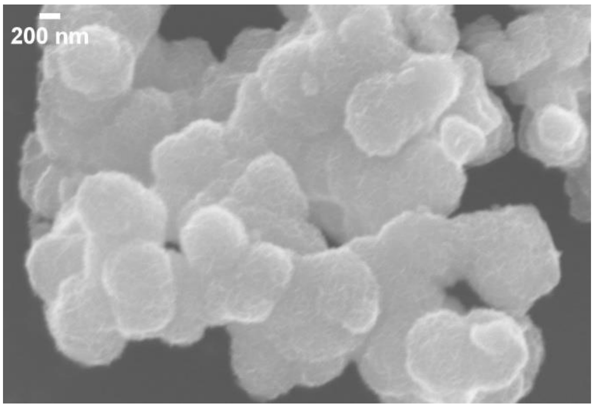


**Figure S8**. FESEM image of NMO after 500 GCD cycles

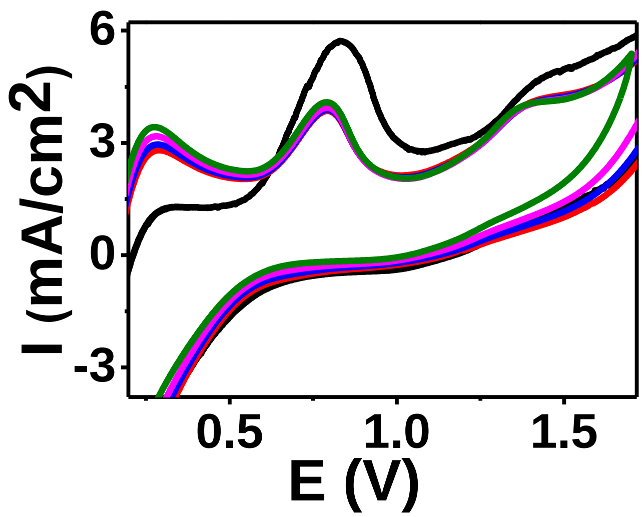


**Figure S9.** The zoomed portion of the CV plot recorded at 60 mA/cm$^2$ at different operating potential windows.

| Sl. No. | Material | Specific capacitance of electrode | Energy density of device | Power density of device | References |
|---|---|---|---|---|---|
| 1 | $Mn_{.95}Co_{.05}O_2$ | 365 F/g | 2.62 µWh/cm$^2$ | 900 µW/cm$^2$ | 1 |
| 2 | $K^+$ intercalated $MnO_2$ | 333.3 $Fg^{-1}$ | 85.2 $Whkg^{-1}$ | 360 W $kg^{-1}$ | 2 |
| 3 | Ni-doped $MnO_2$ nano-array@ carbon cloth | 1398.8 mF $cm^{-2}$ | 0.6871 mWh $cm^{-3}$ | 31.43 mW $cm^{-3}$ | 3 |
| 4 | Na-$MnO_{2-x}$ | 376 F/g | 510.3 mWh $cm^{-3}$ | 40,483 mW $cm^{-3}$ | 4 |
| 5 | Ni-$WS_2$-ACC | 264 F $g^{-1}$ | 22.4 $Whkg^{-1}$ | 803 W $kg^{-1}$ | 5 |
| 6 | 10% Ni-doped $MoS_2$ | 642.07 mF $cm^{-2}$ | 0.00003 Wh/cm$^2$ | 0.0048 W/cm$^2$ | 6 |
| 7 | $MnO_2$-Ni electrode | 325.8 F/g | - | - | 7 |
| 8 | PEDOT-$MoO_3$ | 365 $Fg^{-1}$ | - | - | 8 |
| 9 | 2% Ni-doped $MnO_2$ | 338.1 $Fg^{-1}$ | 6.83 Wh $kg^{-1}$ | 100 W/kg | 9 |
| 10 | 5% Ni-doped $MnO_2$ | 379 $Fg^{-1}$ | 114.6 Wh $kg^{-1}$ | 3600 W $kg^{-1}$ | 10 |
| 11 | reduced graphene oxide decorated Ni doped δ-MnO2 | 217 F/g | - | - | 11 |
| 12 | $Co_3O_4$//$WO_3$ | - | 8 $mWhcm^{-2}$ | 4 mW $cm^{-2}$ | 12 |
| **13** | **1.2 at.% Ni-doped $MnO_2$** | **757.5 mF/cm$^2$ (378.75 F/g)** | **28 mWh/cm$^2$ (6.922 Wh/kg)** | **6056 mW/cm$^2$ (1514 W/kg)** | **This work** |

**Table S1**. Performance comparison of the NMO electrode and ASWSC device with previously reported materials.

## References


1 A. P. Dharani, G. Hariharan, M. Raja, P. Rajeshwaran and S. Kumaran, *J. Mater. Sci. Mater. Electron.*, 2023, **34**, 1–16.

2 L. Xu, G. Pan, J. Wang, J. Li, Z. Gong, T. Lu and L. Pan, *Sustain. Energy Fuels*, 2022, **6**, 5290–5299.

3 R. Zhong, M. Xu, N. Fu, R. Liu, A. Zhou, X. Wang and Z. Yang, *Electrochim. Acta*, 2020, **348**, 136209.

4 B. Thanigai Vetrikarasan, A. R. Nair, S. K. Shinde, D. Y. Kim, J. M. Kim, R. N. Bulakhe, S. N. Sawant and A. D. Jagadale, *J. Energy Storage*, , DOI:10.1016/j.est.2024.112457.

5 K. Pandey and H. K. Jeong, *J. Alloys Compd.*, 2024, **1008**, 176784.

6 A. Panghal, D. Sahoo, D. Deepak, S. Deshmukh, B. Kaviraj and S. S. Roy, *ACS Appl. Nano Mater.*, 2024, **7**, 5358–5371.

7 B. Tan, N. Chen, L. Huang, X. Gao, L. Tan and H. Feng, *J. Ind. Eng. Chem.*, , DOI:10.1016/j.jiec.2024.06.041.

8 S. Muduli, T. K. Pani, K. K. Garlapati and S. K. Martha, *J. Energy Storage*, 2024, **95**, 112396.

9 V. T. Rathod, N. V Brahmankar, Y. Kumar, S. P. Mardikar, G. N. Chaudhari, A. B. Bodade and S. J. Uke, *Inorg. Chem. Commun.*, 2024, **166**, 112643.

10 S. Yao, R. Zhao, S. Wang, Y. Zhou, R. Liu, L. Hu, A. Zhang, R. Yang, X. Liu, Z. Fu, D. Wang, Z. Yang and Y. M. Yan, *Chem. Eng. J.*, 2022, **429**, 132521.

11 N. D. Raskar, D. V. Dake, V. A. Mane, R. B. Sonpir, M. Vasundhara, K. Asokan, U. Deshpande, R. Venkatesh, V. D. Mote and B. N. Dole, *Mater. Sci. Semicond. Process.*, 2024, **178**, 108451.

12 L. Bansal, S. Kandpal, T. Ghosh, C. Rani, B. Sahu, D. K. Rath and R. Kumar, *J. Mater. Chem. C*, 2023, **11**, 16000–16009.